CellPress

Cell Metabolism
Resource

Cell-Type-Resolved Quantitative Proteomics of Murine Liver

S. Babak Azimifar,[1] Nagarjuna Nagaraj,[1] Juergen Cox,[1] and Matthias Mann[1,*]
[1]Department of Proteomics and Signal Transduction, Max Planck Institute of Biochemistry, Am Klopferspitz 18, D-82152 Martinsried, Germany
*Correspondence: mmann@biochem.mpg.de
http://dx.doi.org/10.1016/j.cmet.2014.11.002

SUMMARY

Mass spectrometry (MS)-based proteomics provides a powerful approach to globally investigate the biological function of individual cell types in mammalian organs. Here, we applied this technology to the in-depth analysis of purified hepatic cell types from mouse. We quantified 11,520 proteins, making this the most comprehensive proteomic resource of any organ to date. Global protein copy number determination demonstrated that a large proportion of the hepatocyte proteome is dedicated to fatty acid and xenobiotic metabolism. We identified as-yet-unknown components of the TGF-β signaling pathway and extracellular matrix in hepatic stellate cells, uncovering their regulative role in liver physiology. Moreover, our high-resolution proteomic data set enabled us to compare the distinct functional roles of hepatic cell types in cholesterol flux, cellular trafficking, and growth factor receptor signaling. This study provides a comprehensive resource for liver biology and biomedicine.

INTRODUCTION

The liver is the metabolic center of the mammalian body. It is the largest internal organ with a complex architecture that ensures the proper interaction of hepatic cell types (HCTs) within the microenvironment of the liver. HCTs perform wide-ranging biological functions such as amino acid, fatty acid, and carbohydrate metabolism; synthesis of bile acids and hormones; lipoprotein biogenesis; and detoxification (Falcón-Pérez et al., 2010). The majority of these physiological tasks are carried out by hepatocytes (HCs), the hepatic parenchyma that occupies approximately 90% of liver volume. The remaining, "nonparenchymal" cells (NPCs) are Kupffer cells (KCs), which are hepatic macrophages; liver sinusoidal endothelial cells (LSECs), which line the blood vessels; hepatic stellate or Ito cells (HSCs), which are involved in liver fibrosis; intrahepatic cholangiocytes (CHCs); epithelial biliary tree cells; and other rare cell types. The isolation of HCTs with high purity and quantity is challenging due to several technical obstacles, including low isolation yield of rare NPCs as well as controversy over cell-type-specific markers (Elvevold et al., 2008). In recent years, protocols have been developed to optimize the isolation of HCTs (Liu et al., 2011; Maschmeyer et al., 2011); however, they have not yet been applied to investigate functional specialties of all HCTs in a single study.

Mass spectrometry (MS)-based proteomics provides a unique and powerful means of investigating proteomic signature of biological samples in an unbiased manner (Aebersold and Mann, 2003). Difficulties facing proteomic studies of the liver include the high complexity of the hepatic proteome and the very high abundance of metabolic enzymes that can preclude coverage of low abundant proteins. Moreover, the liver contains a large volume of circulating blood that can dramatically affect proteome coverage and quantification. Early studies were performed by 2D gel electrophoresis and generally only identified a few hundred proteins (Iida et al., 2003; Li et al., 2004). Liquid chromatography-tandem mass spectrometry (LC-MS/MS)-based proteomics has been applied to the liver proteome, but such studies were initially limited to between 2,000 to 3,000 identified proteins (Shi et al., 2007; Yan et al., 2004). The "Liverbase," a public database of the Human Proteome Organization (HUPO), summarized these studies and currently comprises 6,788 proteins of adult human liver in healthy and altered physiological conditions (Sun et al., 2010). The essential role of the liver in whole-body physiology and the relatively easy access to large amounts of hepatic lysates make it an attractive organ not only for expression proteomic studies of the homogenized organ but also for subcellular structures (Falcón-Pérez et al., 2010) as well as for the analysis of posttranslational modifications (Monetti et al., 2011; Okabe et al., 2009).

Recently, substantial improvements in the entire MS-based proteomics pipeline, including sample preparation, liquid chromatography, and mass spectrometry hardware, as well as data analysis, have enabled nearly compete proteome coverage of cell lines (Mann et al., 2013). A recent liver proteomics data resource contains 7,700 unique UniProt identifications, as well as many protein variants (Low et al., 2013). Despite progress in HCTs isolation techniques, proteomics studies of the liver to date have been restricted to total liver homogenate that is vastly overshadowed by the proteome of HCs. However, many hepatic processes, which occur through intercellular signaling crosstalk mechanisms, cannot be investigated by data obtained from mixed cell populations (Bohm et al., 2010), necessitating in-depth and cell-type-resolved proteomic analysis of the liver.

In this study, we obtained highly purified HCTs of murine liver using a combination of density gradient centrifugation and magnetic affinity cell sorting techniques. We subsequently applied the recently developed "in-StageTip" (iST) sample preparation method (Kulak et al., 2014) and an advanced LC-MS/MS

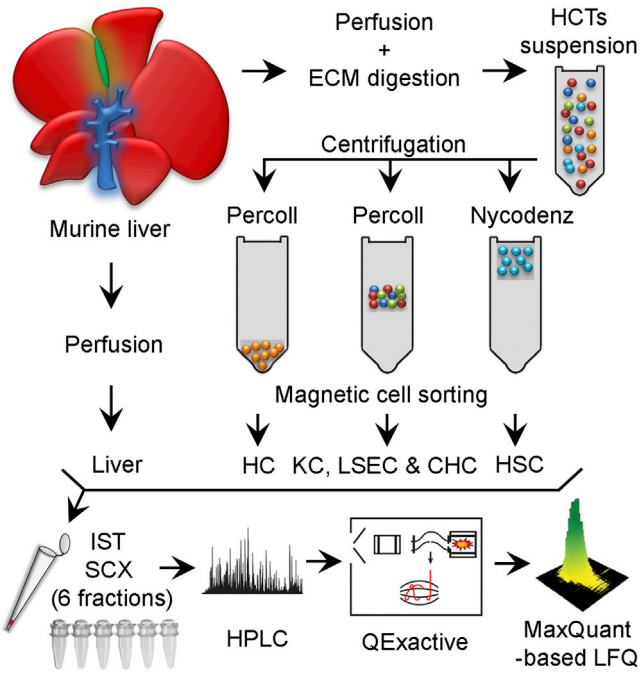

Figure 1. Proteomic Analysis of HCTs
Schematic workflow for the cell-type-resolved proteomics of murine liver.

workflow for in-depth profiling, analysis, and comparison of the proteomes of five hepatic cell types. Our results provide a comprehensive and quantitative proteomic data source for individual cell types of a mammalian organ.

RESULTS

In-Depth Quantitative Proteomics of HCTs

To generate a cell-type-resolved proteomic atlas of the mouse liver, we isolated the five HCTs from male adult murine livers using a two-step purification approach (Figure 1; Experimental Procedures). We achieved highly purified populations of HCTs with values for HCs, KCs, LSECs, HSCs, and CHCs in excess of 99%, 97%, 96.5%, 98%, and 93.5%, respectively (Figure S1 available online). The purified HCTs and blood-free perfused liver were processed using the recently published iST method, which drastically reduces sample processing steps by confining lysates to a single vessel (Kulak et al., 2014). We chose a six-fraction elution with strong cation exchange (SCX) prefractionation steps to achieve in-depth proteome coverage with reasonable measuring time and high sensitivity. The entire proteomic experiments were performed as biological quadruplicates for the HCT proteome measurements and as biological triplicates for the primary HCs dedifferentiation experiments (Experimental Procedures). To further increase proteome coverage, we transferred peptide identifications from a "peptide library" of three distinct mouse cell lines (Hepa 1-6, Hep-53.4, and J774.2) using the "match between runs" feature implemented in MaxQuant (Cox and Mann, 2008). The resulting 27 proteome samples were analyzed by high-resolution LC-MS/MS using 4 hr gradients on a benchtop Orbitrap mass spectrometer (Q Exactive), generating 162 measurement runs containing nearly 15 million high-resolution MS/MS spectra. All data files were processed by the MaxQuant computational environment with >99% confidence at both protein and peptide levels (false discovery rate [FDR] < 1%) for identification by the Andromeda search engine (Cox et al., 2011). Label-free quantification in MaxQuant is based on accurate detection of eluting peptides as 3D objects in mass to charge ratio (m/z), elution time, and signal intensity space. The peak intensities for the same peptides are compared to each other across conditions, and variations in mass spectrometric sensitivity between measurements are minimized by sophisticated normalization algorithms (Cox et al., 2014).

In total, we quantified more than 11,520 proteins, creating the largest and most accurate organ proteomic resource to date (Figure 2A; Table S1). Of these, 8,338 proteins (72%) were detected in all experiments, revealing that the majority of the proteome is expressed in all cell types (Figure S2A). Our label-free quantitative data were highly reproducible among the biological replicates and showed an average Pearson correlation coefficient of 0.96 (Figure S2B). ANOVA revealed that at least 59% of quantified proteins were differently expressed between HCTs (FDR < 0.01; 6,778 proteins; Figure 2B). This demonstrates that despite the ubiquitous expression of the majority of the proteome between cell types, there are substantial quantitative specializations of individual cell-type proteomes that enable the execution of the appropriate physiological functions. One technical advantage of cell-type-specific analysis is the concomitant reduction in dynamic range. Indeed, we observed that over 10% of total quantified proteins were uniquely quantified in HCTs, but not in total liver sample (1,230 proteins; Figure 2B). To analyze and compare the dynamic range of these proteomes, we used the protein intensities derived from summed peptide intensities and the cumulative protein abundance of measured samples (Figures 2C, S2C, and S2D; Experimental Procedures). The broadest proteome dynamic range was found in HCs and total liver, spanning nearly seven orders of magnitude (Figure 2C). The top 100 most abundant proteins in HCs and total liver are almost identical, and these top 100 proteins alone comprised over 40% of the mass of the total proteomes (Figures S2C and S2D), highlighting the wide dynamic range in protein abundance in the liver proteome. The majority of these abundant proteins were metabolic enzymes of different biological processes, emphasizing the prominent role of liver as the metabolic center of the body. The entire cell-type-specific proteome of liver can easily be visualized in the MaxQB database (Schaab et al., 2012).

Comparison of Proteomics and RNASeq Data in Liver

To determine the relationship between transcriptome and proteome for murine liver and to assess the depth reached by our workflow, we compared our quantitative proteome of liver sample with a transcriptome obtained by RNA sequencing (Mortazavi et al., 2008). We mapped the RNASeq data to 16,589 protein-coding genes based on the UniProt Knowledgebase (UniProtKB) (Magrane and Consortium, 2011). To estimate absolute protein amounts, we first used iBAQ values, which represent the protein abundance normalized to the number of theoretically observable peptides (Schwanhäusser et al., 2011). A total of 91% of all genes detected by RNASeq and passing the commonly used cutoff value of RPKM > 1.0 had corresponding

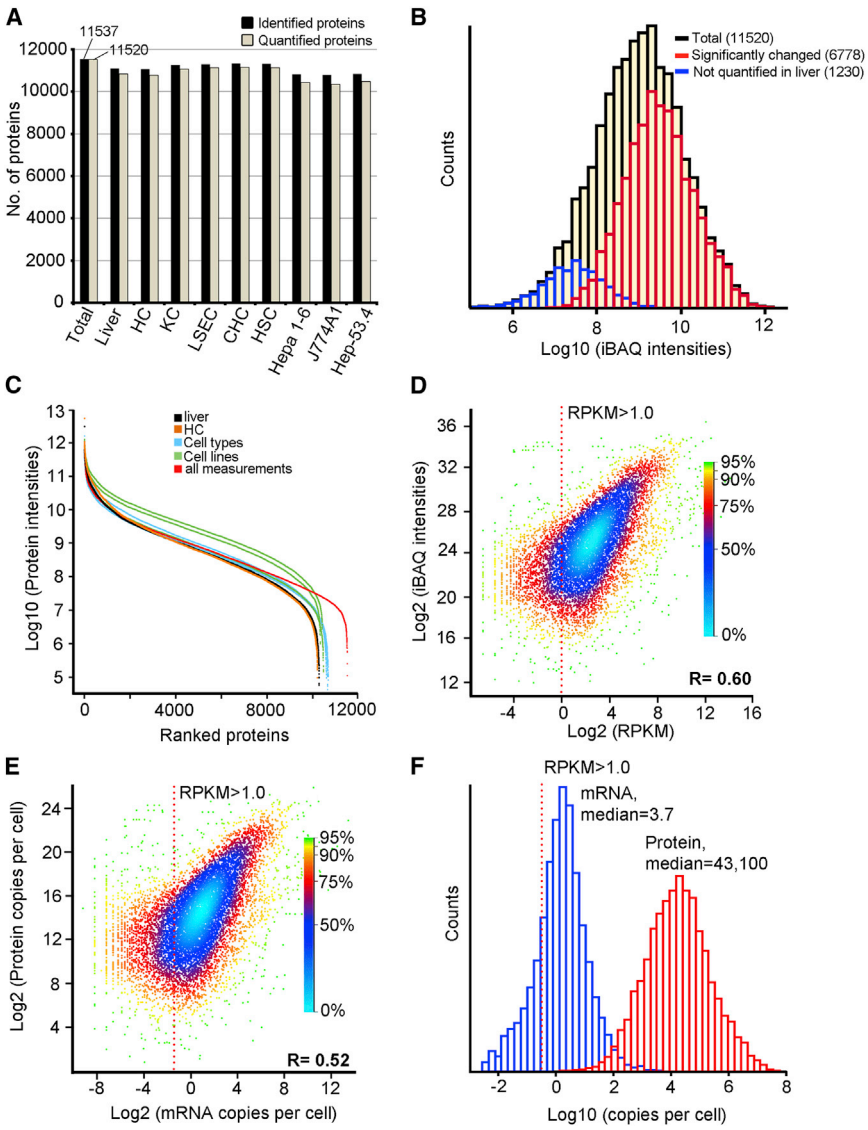

Figure 2. In-Depth Proteome Coverage of HCTs

(A) Identified and quantified proteins in different cell types. Hepa 1-6, Hep-53.4, and J774.2 were the mouse cell lines that we used for generation of the peptide library (Experimental Procedures).

(B) Distribution of all quantified proteins (11,520; black), significantly changed protein among HCTs (6,778 proteins, ANOVA, FDR < 0.01; red), and proteins only quantified in HCTs but not liver (1,230; blue).

(C) Dynamic range of the proteomes of measured samples, based on raw protein intensities.

(D) Comparison of protein intensities versus mRNA intensities for total liver.

(E) Comparison of protein copy numbers versus mRNA copy number for total liver.

(D and E) The color code represents the density of points in the corresponding region.

(F) Distribution of the mRNA (blue) and protein (red) copy numbers for total liver. The red dashed-lines indicate the threshold for robust transcription detection (RPKM > 1.0) (Mortazavi et al., 2008).

iBAQ values in the proteome (Figure S2E). Reported global correlations between transcriptome and proteome are typically in the range of 0.4–0.6 (Low et al., 2013; Nagaraj et al., 2011), implying that proteome variations can only be explained by transcript levels to a limited degree (Schwanhäusser et al., 2011). For the nearly 8,311 RNA-protein matches (RPKM > 1.0), we obtained a correlation of 0.60 between RNASeq and our iBAQ values (Pearson correlation coefficient, R = 0.60; Figure 2D). The correlation was 0.52 when we calculated protein-RNA copy numbers from the same data sets (R = 0.52; Figure 2E) on the basis of individual protein intensities (Wiśniewski et al., 2014). These transcriptome-proteome correlations were stronger than the correlations of about 0.43 reported for the liver of two rat strains (Low et al., 2013). The copy number range of liver proteins spanned approximately seven orders of magnitude. Reflecting the generally lower amounts of mRNA in tissue, we found that the reported mRNAs copy numbers (Mortazavi et al., 2008) were on average approximately 10,000-fold lower than protein copy numbers (Figure 2F).

Transformation of Primary HCs in Tissue Culture

Freshly isolated primary HCs undergo rapid dedifferentiation toward cell line phenotype in tissue cultures over a period of days. However, the proteomic transformation associated with this process has not been investigated in great depth and never along a time course (Pan et al., 2009). To investigate this process, we quantified the proteome of freshly isolated primary HCs, HCs that we harvested from 1-, 3-, and 7-day cultures as well as the Hepa 1-6 cell line (Figures 3 and S3; Table S2). The experiment was performed in biological triplicates in less than 1 week of measuring time, resulting in quantification of 10,305 proteins over the course of transformation. The reproducibility among replicates was high with an average Pearson correlation coefficient of about 0.99 (Figure S3A). Approximately 35% of the primary HCs proteome changed significantly over the 7 day time course in tissue culture (3,427 proteins, t test, $p < 0.01$; Figure 3A), indicating substantial proteome remodeling. Interestingly, the dynamic range of the proteomes as visualized by the iBAQ values gradually contracted toward the range typical of cell lines in an orderly manner (Figure 3B). Likewise, the proteome correlation between primary HCs and cultured HCs or Hepa 1-6 cell line showed a progressive decrease in proteome similarities (Figure 3C). The gradual transformation of primary HCs in cell culture was also clearly captured by principle component analysis of the proteomes (Figure 3D). The partners of the complement system, including Complement factor H (CFH), Complement C3 (C3), and Complement C4-B (C4-B), as well as Asialoglycoprotein receptor proteins 2 (ASGR-2, a subunit of Ashwell-Morell receptor), decreased gradually in tissue culture and in the Hepa 1-6 cell line (Figures S3B).

This suggests a decrease in the ability of primary HCs to clarify cell debris and particles from their microenvironment (Ricklin and Lambris, 2007; van't Veer and van der Poll, 2008). Conversely, we observed a gradual increase in the levels of cytoskeletal proteins, Filamin-A, Filamin-C and PDLI7, trafficking proteins annexin-A2 and A3, as well as Astrocytic phosphoprotein PEA-15, which regulated ERK1/2-dependent processes and H-RAS-mediated cell transformation (Figures S3B) (Sulzmaier et al., 2012). These variations in protein levels were mirrored in the expression of their corresponding mRNAs measured by RT-PCR, which also served to independently verify the ability of our proteomic data to capture proteomic variations in target cells (Figure 3E).

Comparing the Proteome Signatures of HCTs

We investigated the global diversity of HCTs by unsupervised hierarchical clustering of all quantified proteomes. The hierarchical matrix was divided into two main groups: one cluster comprising total liver and HCs and a second cluster of NPCs subdivided into KCs, a subgroup of HSCs, and a smaller subgroup of LSECs and CHCs (Figure 4A). This cosegregation was also represented by principal-component analysis (PCA) of HCTs (Figure S3C). The high contribution of HCs to the total liver proteome is in agreement with previous studies (Falcón-Pérez et al., 2010) and the known organization of liver tissue. We next investigated how the global proteome patterns related to the cell lineages of HCTs. The clustering and PCA patterns from our data confirmed the distinctive hematopoietic fate of KCs, while the cosegregation of HSCs with LSECs suggests a similar mesodermal origin for both cell types based on their global proteome compositions. The embryonic lineage of HSCs has been controversial, with an origin in all three germ layers having been proposed before (Yin et al., 2013) (Figures 4A and S3C). We filtered our data for gene and protein annotations that were enriched in the three prominent clusters observed in Figure 4 (Fisher exact, FDR < 0.02 after Benjamini-Hochberg correction; Figures 4A and 4B; Table S3). The enrichment of MHC-II and asthma annotations in KCs, resident macrophages of liver, is in line with their physiological role in innate immune responses and inhibition of inflammatory cytokine (Thomson and Knolle, 2010). These results demonstrate that our proteomic resource recapitulates the key physiological functions of HCTs in an unbiased manner and that they can serve as a valuable data source for future investigations into hepatic cell type functions.

Cell-Type-Specific Protein Expression in Murine liver

To identify proteins that display cell-type-specific expression profiles, we filtered our quantitative data for proteins that were only detected in one cell type or showed at least 30-fold higher expression levels in one of the HCTs (ANOVA, FDR < 0.01; Figure 4C; Table S4). We compared our list of HC- and KC-specific protein candidates by assessing immunostained liver sections in the Human Protein Atlas (Uhlen et al., 2010) (Figures S4A and S4B). For example, the S100A9 protein, which has been shown to promote inflammation and systemic autoimmunity (Loser et al., 2010), was specifically abundant in KCs and showed a corresponding KC-specific immunostaining in liver sections (Figure S4B). We performed a Fisher exact test for all the proteins that significantly changed among the HCTs, and as expected, many metabolic processes were enriched with very significant p values (Fisher exact, FDR > 0.02; Table S5). We next explored the contribution of individual HCT to the liver proteome by comparing the quantified proteomes in each HCT versus total liver (t test, FDR 0.01 and 0.001) (Figures 4D, 4E, and S4C–S4E; Table S6). Comparison of the proteome of HCs with the liver revealed that the few significantly represented proteins in the liver sample were mostly components of the extracellular matrix, as expected when comparing homogenized organ to individually enriched cells (Figure S4E). Conversely, the proteome of the NPCs contained specific proteins not detected in total liver, confirming the importance of cell-type resolution in creating an accurate and complete atlas of this organ.

Comparison of the proteome of HCs (liver parenchyma) against the median of quantified proteins in all liver NPCs (Figure S4F; Table S6) provided a detailed picture of the variation of proteome profiles between parenchymal cells and NPCs of this organ. For example, a known marker of KCs, a subunit of macrophage-1 antigen (integrin αm) (Larson and Springer, 1990), was significantly represented in NPCs, while the levels of Ashwell-Morell receptor (consisting of combinations of the Asialoglycoprotein receptor proteins, ASGR-1 and -2) (van't Veer and van der Poll, 2008) was prominent in HCs. In general, these protein profiles reflect the global organization of proteomes in hepatic parenchymal cells and NPCs, which modulate metabolic and specialized (patho)physiological processes in the liver.

Proteomic Functional Hotspots in HCTs

We next sought to mark functional hotspots of HCT proteomes through estimation of the absolute amount of proteins in all HCTs (Wiśniewski et al., 2014). The three most abundant proteins in HCs were liver-specific fatty acid binding protein 1 (FABP1), glutathione S-transferase P (GSTP1), and the mitochondrial enzyme carbamoyl-phosphate synthase (CPS1), highlighting the important role of liver parenchyma in fatty acid metabolism, xenobiotic biodegradation, and urea cycle (Figures 5A–5C). In contrast, the top most abundant proteins in all hepatic NPCs were histone core proteins (Table S7A). We also observed highly abundant proteins that were specific to NPCs and were known to be involved in specialized cellular functions. For example, KCs contained high levels of S100A8 and S100A9, calcium-binding proteins that have been reported to promote inflammation and autoimmune response via Toll-like receptor 4 signaling (Loser et al., 2010). Components of the cytoskeleton and actomyosin machinery, including the α-actins, transgelin, destrin, filamin-A, tropomyosins, and myosins, were highly represented especially in LSECs. These proteins sense and transduce mechanical forces and support cellular structure and integrity in other endothelial cells, which have to tolerate high mechanical stress (Tojkander et al., 2012). HSCs were highly enriched for specific trafficking proteins, including annexin-2 and -3; sorting nexin-2, -3, and -5; and Rab-7 and -11, indicating the importance of specialized intracellular trafficking in HSCs. Moreover, annexin-A5 and -A4, as well as prothymosin-α and parathymosin, were specifically abundant in CHCs (Table S7A). CHCs are the first line of immune defense in the biliary system, and the expression of prothymosin-α and parathymosin protect against opportunistic infections in liver (Hannappel and Huff,

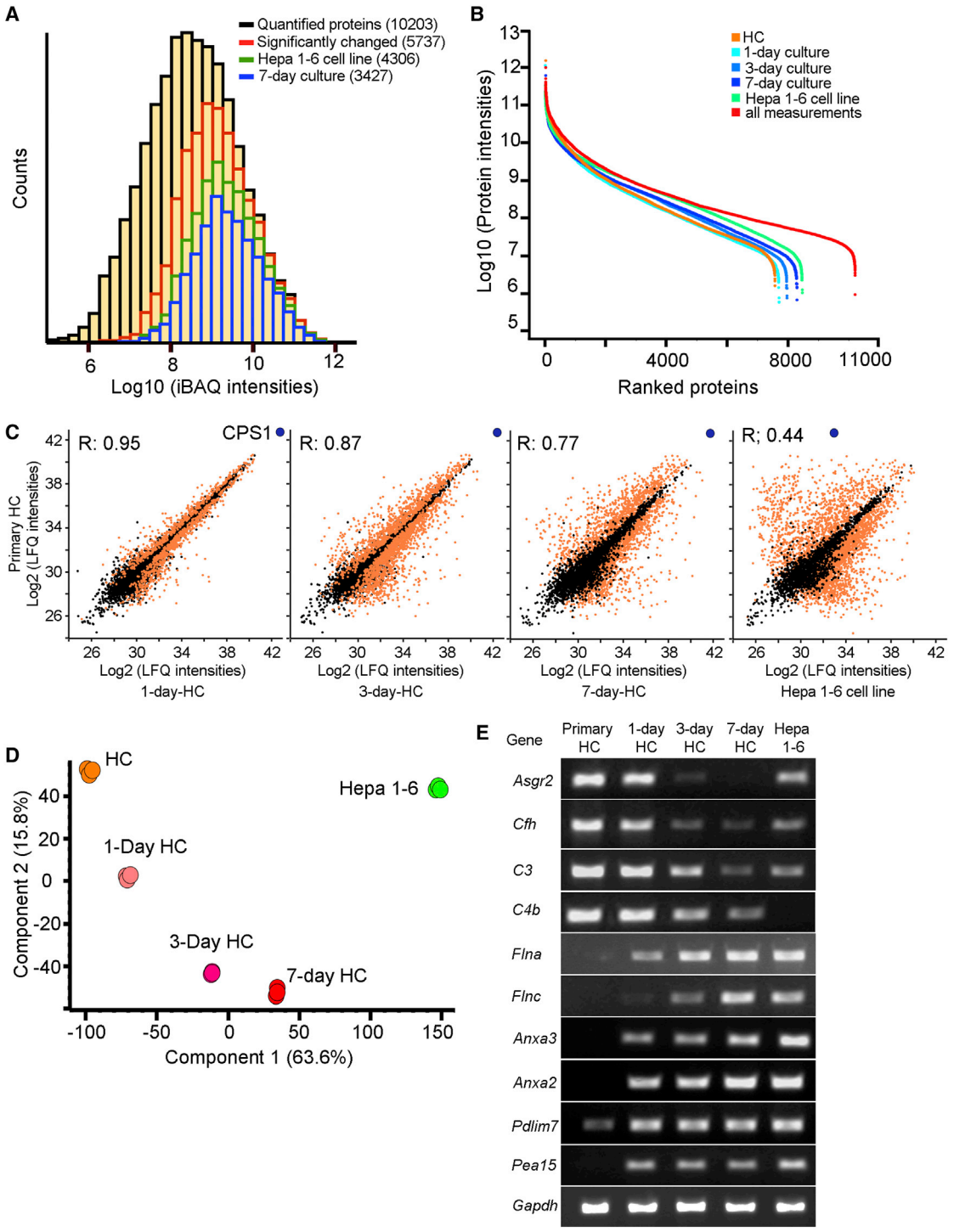

Figure 3. Dedifferentiation of Primary HCs in Tissue Culture

(A) Distribution of all quantified proteins (10,203; black), significantly changing proteins over the dynamic proteome evolution (5,737, ANOVA, FDR < 0.01; red), and significantly changed primary HC proteins in Hepa1-6 cell line (4,306, t test, $p < 0.01$; green) and in 7-day cultures of primary HC (3,427, t test, $p < 0.01$; blue).

(B) Gradual change in the dynamic range of the proteome from freshly isolated primary HCs to primary HCs cultured for 1, 3, and 7 days and to the Hepa 1-6 cell line.

(C) Gradual decrease in proteome similarity during proteome evolution toward cell line behavior. R is the Pearson correlation coefficient. Brown dots indicate significantly changed primary HC proteins (t test, $p < 0.01$). Blue dot represents mitochondrial CPS1, which triggers the first enzymatic reaction of the urea cycle. The expression level of CPS1 was extremely high in primary HCs and decreased dramatically in the Hepa 1-6 cell line.

(legend continued on next page)

2003; Syal et al., 2012). We next used copy number ranking to assess the enriched gene and protein annotations in the individual HCT proteomes (Fisher exact test, FDR < 0.01; Tables S7A–S7F). We visualized different protein classes enriched in various abundance quantiles of HCs and HSCs as representative examples (Figures 5D and 5E). Annotations of basic cellular process including the respiratory chain and proteasome core complex were ubiquitous in all HCTs. In contrast, HCs were highly specialized for the major physiological functions of liver, emphasizing their prominent role as hepatic parenchyma. The "intraflagellar transport particle A" and "anchored to membrane" terms were exclusively enriched in the low-abundance quartile of HCs and HSCs, respectively. Less is known about the physiological function of HSCs compared to other HCTs in normal liver (Yin et al., 2013). We therefore utilized our in-depth quantitative data to highlight molecular players of ECM assembly, cytoskeleton, transforming growth factor β (TGF-β) signaling pathway, and immune response in HSCs (Figure 5F; Table S8). This illustrates the usefulness of our copy number catalog of HCTs for functional descriptions as well as their potential for guiding future studies into liver cell biology.

System-Wide Proteomic Profiling of Biological Process in Murine Liver

We next sought to globally define the individual physiological roles of HCTs in the liver tissue from the comparative proteome profiling data. The liver centrally regulates cholesterol levels in the body. The protein expression profiles of the cell types indicate that not only HCs but also KCs and CHCs appear to be involved in cholesterol recycling (Figure 6). The role of CHCs in cholesterol flux is less appreciated, but it is known that they play a crucial role in the inhibition of biliary disease and gallstone formation (Xia et al., 2012). The Ashwell-Morell receptor (consisting of combinations of the Asialoglycoprotein receptor proteins, ASGR-1 and -2) is highly expressed in liver and is responsible for rapid clearance of asialoglycoproteins, von Willebrand factor, and platelets from circulating blood (van't Veer and van der Poll, 2008). In agreement with previous studies (Lee et al., 2009; van't Veer and van der Poll, 2008), Ashwell receptor is predominantly expressed in HCs (Figure S5A). Interestingly, the ratio of copy numbers of ASGR1 to ASGR2 was approximately 4:1 in HCs, 5:1 in KCs, and 7:1 in LSECs (Table S7A), suggesting that the ASGR-1/-1/-2 trimer is not the only oligomeric combination of Ashwell receptors (van't Veer and van der Poll, 2008). While these receptors and peroxisomal proteins are highly expressed in HCs (Figures S5A and S5B), our data indicates that LSECs, HSCs, and CHCs more actively participate in caveolae-mediated uptake, clathrin-mediated endocytosis, and membrane trafficking (Figures S5C–S5F). High expression levels of proteins involved in clathrin- and caveolae-mediated uptake in CHCs (Figures S5C and S5D) would facilitate cholesterol transfer through SR-BI, LDLR and CD36 receptors (Röhrl and Stangl, 2013). Moreover, the internalization of the Ashwell receptor is coupled to clathrin-mediated endocytosis or transcytosis. The high expression levels of this machinery in LSECs and KCs could also actively contribute to the previously reported intravascular blood clearance of platelets during sepsis (van't Veer and van der Poll, 2008).

The Profile of Cell Signaling Receptors in HCTs

To assess the completeness of our data and the potential of the different HCTs to trigger signaling pathways through cell surface receptors, we annotated a list of receptor tyrosine kinases, growth factor (GF) receptors, and their main coreceptors by integrating data from the UniProtKB database and the literature. We compared this list with our atlas of liver proteins, as well as proteins annotated as hepatic in UniProtKB and a liver RNASeq analysis (Mortazavi et al., 2008) (Table S9). Of these data sets, ours had the largest coverage, encompassing 115 receptors, including 40 not identified in the two other data sets (Figure 7A). We assessed our quantitative data (Table S1) for the expression profiles of several well-known GF receptors in HCTs (Figure 7B). HCs expressed the highest levels of epidermal GF receptors ErbB1 and ErbB3 (EGFR and HER3), but not ErbB2. We did not detect TβRIII (β-glycan) receptors in HCs, in agreement with previous findings in rat (Date et al., 2000; Scheving et al., 2006). Only HSCs expressed platelet-derived growth factor receptor alpha (PDGFRA) receptor, and these cells also showed the highest levels of TGF-β receptors (TβRI to -III), indicating the diversity of stimuli that can stimulate HSCs (Figure 7B). The TβRI:TβRII receptor was present in all HCTs, except LSECs, in which we did not detect expression of TβRI (Figure 7B). As demonstrated by these examples, our atlas of copy numbers can be used to illuminate and place constraints on possible signaling mechanisms in liver cell types.

DISCUSSION

Transcriptomic, proteomic, and metabolomic studies of mammalian organs have typically been performed on tissue homogenates, while the few cell-type-specific studies have generally focused on just a small subset of cell types. Here we provide the first comprehensive and cell-type-resolved organ proteomic atlas and show how in-depth and quantitative cataloging of tissue proteomes can directly shed light on functional specialization of the different liver cell types. Furthermore, the deep proteome data provided here can complement liver metabolomics efforts by making it possible to correlate changes in metabolites with changes of enzyme levels on a global scale.

We here achieved a deep and nearly complete proteome coverage of liver with more than 11,520 identified and quantified proteins through our recently developed streamlined MS-based proteomics pipeline (Kulak et al., 2014; Mann et al., 2013). This proteome coverage is remarkable considering the complexity of the liver proteome and wide dynamic range of the liver, particularly of the HCs. Recent reports on human liver proteome also led to identification of 10,221 and 9,385 of

(D) PCA showing that the overall proteomic phenotype smoothly changes during culturing in the first dimension, whereas the cell line is separated from primary cells in the first but not the second PCA dimension. Each spot represents one biological replicate.
(E) RT-PCR for candidate proteins that were significantly changing over the dynamic proteome transformation shows the same dynamics as the corresponding protein changes (Figure S3B).

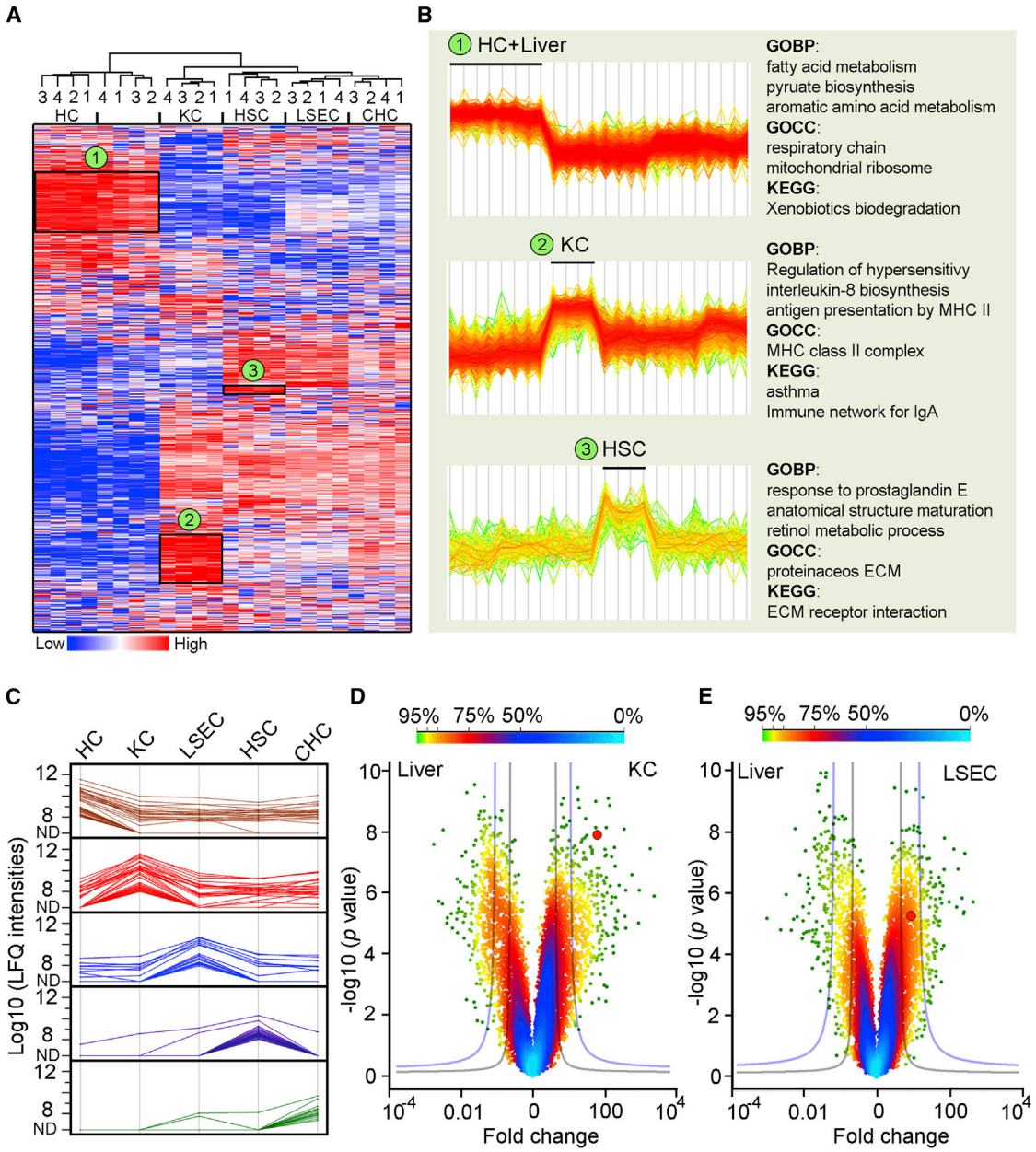

Figure 4. Cell-Type-Specific Expression Profiles of Murine Liver

(A) Unsupervised hierarchical clustering of quantified proteomes. HCs and total liver segregates from NPCs cell types. Numbers above each cell types indicate the replicates. Numbers indicate enriched clusters of proteins in HCs and liver (1), KCs (2), and HSCs (3).

(B) Enriched annotations for corresponding clusters in Figure 3A (Fisher exact test, FDR < 0.02 after Benjamini-Hochberg correction).

(C) Protein expression profiles of cell-type-specific proteins that were highly expressed in specific HCTs (ANOVA, FDR < 0.01). "ND" indicates "Not Detected."

(D) Proteome comparison between liver and KCs. The red circle indicates integrin αm, which forms the CD11b receptor of KCs, a specific KC marker.

(E) Proteome comparison between liver and LSECs. The red circle represents, Stab2, a specific LSECs marker.

(D and E) Gray and violet lines indicate significance thresholds of 0.01 and 0.001, respectively. The color code represents the density of points in the corresponding region.

unique UniProt identifications from total adult- and fetal-liver homogenates, respectively (Kim et al., 2014). However, these livers also contained blood, and recently, it has been concluded that due to poorly identified peptide and low-quality of spectra, these data overestimate the number of protein and should be considered with caution (Ezkurdia et al., 2014; Wilhelm et al., 2014). The top 100 most abundant proteins in HCs and the liver alone comprised more than 40% of the total copies of protein in the proteome (Figure S2C). This is in line with a study showing that the top 100 mRNAs in liver constitute approximately 50% of the total transcriptome (Ramsköld et al., 2009).

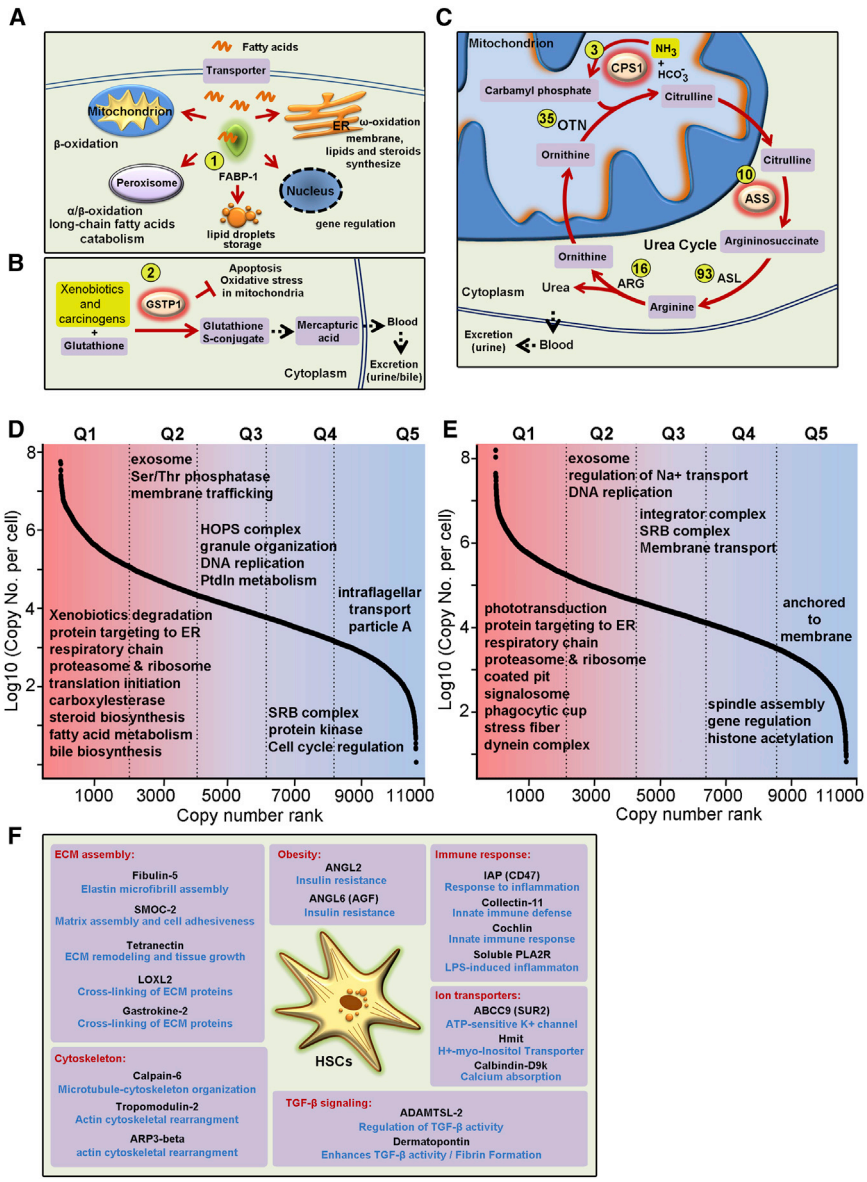

Figure 5. Proteomic Functional Hotspots of HCs

(A–C) A schematic representation of the molecular functions of top ranking proteins expressed in HCs. The numbers in yellow circles indicate the copy number ranks.

(A) Liver fatty-acid-binding protein (FABP-1) is involved in the trafficking of fatty acids to different subcellular structures (including mitochondria, peroxisomes, and endoplasmic reticulum [for lipid metabolism]), to lipid droplets (for storage), and to the nucleus for lipid-mediated transcriptional regulation.

(B) Glutathione S-transferase P1 (GSTP1) catalyzes the conjugation of xenobiotics and carcinogens to glutathione that eventually leads to the production of mercapturic acids and excretion via urine and bile. GSTP1 also inhibits apoptosis and oxidative stress in mitochondria.

(C) Mitochondrial CPS1 mediates the detoxification of ammonia via the transfer of the ammonia group in the urea cycle, enabling its excretion into the blood. This is achieved by the synthesis of carbamoyl phosphate. Many other proteins of the urea cycle also showed high expression levels in HCs.

(D and E) Ranked protein copy numbers in (D) HCs and (E) HSCs. Proteins were divided to five abundance quartiles. The top most significantly enriched annotations in each quartile are indicated (Fisher exact test, FDR < 0.01 after Benjamini-Hochberg correction).

(F) The list of proteins with exclusively higher copy numbers in HSCs. The proteins were grouped based on their role in different biological process (Table S8).

Calculating protein copy numbers per cell in liver, we found that, on average, hepatic proteins are 10,000 times more abundant compare to their coding mRNA (Figure 2F). Interestingly this is somewhat larger than the recently reported protein-mRNA abundant ratio of 2,800 for NH3T3 cell line (Schwanhäusser et al., 2011). This may reflect the fact that dividing cell lines have more need for mRNA biosynthesis than postmitotic tissues, which are also likely to express a great abundance of structural and enzymatic proteins.

The origin of the HSC lineage is controversial, with genetic studies in cell lines and mice supporting a mesodermal origin and studies of human fetal liver showing expression of endodermal markers (Yin et al., 2013). On the other hand, there are reports of a mesenchymal origin from bone-marrow-derived cells, and an epithelial-mesenchymal transition in injured livers could contribute to HSCs (Miyata et al., 2008). In line with the abovementioned genetic studies, the pattern of cosegregation of HSCs with LSECs in statistical analyses from our quantitative data supports a mesodermal origin for HSCs (Figures 4A and S3C).

We explored the contribution of protein expression of individual HCTs to the total liver tissue (Figures 4D, 4E, and S4C–S4E). The proteomic signature of HCTs represents the physiological function of each cell type in liver, and therefore, these results allow molecular dissection of underlying biological process in liver. Although we provided the cell-type-specific proteome signature of liver, we note that distinct perivenous and periportal hepatic populations exist, which we have not yet analyzed. If they can be efficiently purified, they would be an interesting topic for further proteomic studies.

Applying our technology to a dynamic process, we did, however, already explore the proteome transformation of primary HCs in culture. The question of how close cell lines are to primary cells and how the latter transform into cultured states is a generally important one that has not been addressed before at the proteomics level. Our 7-day time course data revealed that the proteome of primary HCs starts adapting to the in vitro microenvironment as early as 24 hr after isolation from the liver. Moreover, although Hepa 1-6 cell line expressed many characteristics of HCs, they lack key metabolic enzymes and showed a poor

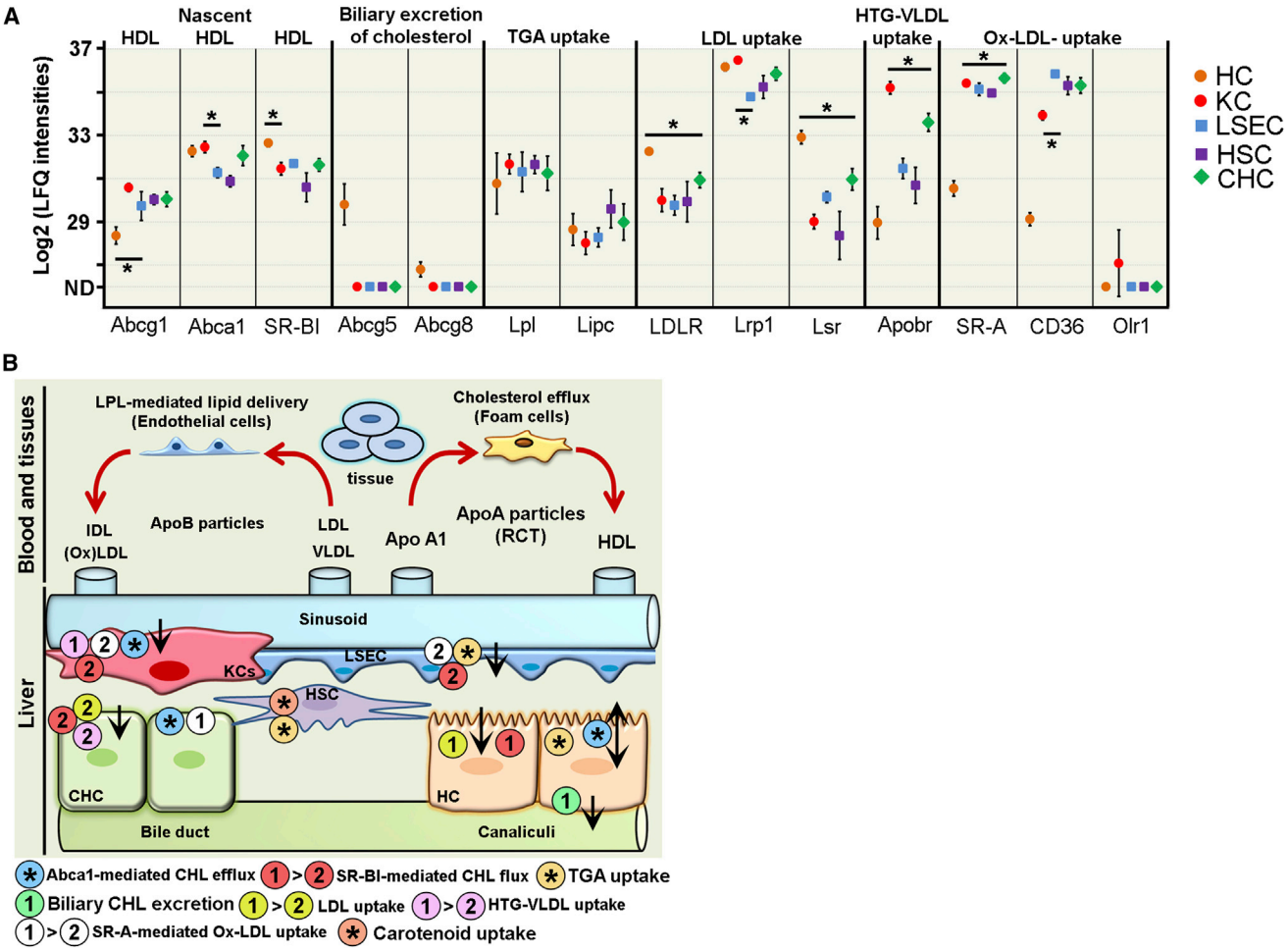

Figure 6. Cholesterol Flux in the Liver

(A) The expression profiles of HCTs were compared for cell surface receptors that are involved in cholesterol flux. Data are median ± SD. Stars indicate t test significance (*$p < 0.05$). "ND" indicates "Not Detected."

(B) Functional contribution of HCTs in cholesterol flux is depicted based on the quantitative data from (A).

(A and B) HCs and KCs displayed higher expression levels of Abca1 and SR-BI, which mediate cholesterol flux with lipoproteins particles (blue stars). Biliary secretion of cholesterol through Abcg5/Abcg8 dimer was restricted to HCS. Triglyceride uptake through Lpl and Lipc was similar between different cell types; however, as HCs and LSECs are the most abundant cell type in the liver, they contribute a bigger role in triglyceride uptake. LDL uptake via LDLR, Lrp1, and Lsr was high in HCs and to a lower extent in CHCs (yellow). KCs showed the highest capacity for the uptake of modified-LDL via Apobr, SR-A, and Olr1. HCs also can uptake oxidized-LDL via LDLR.

correlation in expression levels with the proteome of primary HCs (R = 0.44; Figure 3C). This further emphasizes that although cell lines are powerful in vitro systems to study many biological processes, they can be much different from their corresponding tissues and fresh primary cells. Importantly, our data makes it possible to pinpoint at the proteome level which functions are similar and which are distinct between these cellular states.

We also estimated the copy numbers of the detected proteins in all cell types using our recently developed proteomic ruler concept (Wiśniewski et al., 2014). This analysis revealed proteomic hotspots of HCTs through the marked quantitative differences of individual proteins and pathways in the different cell types. For instance, HCs are known to contain a high number and density of mitochondria and make up an estimated one fifth of the cell volume of HCs (Beauvoit et al., 1994). Our data quantify this notion, and we found that 53 out of the top 100 most abundant proteins in HCs (Figure S2C; 27% of the proteome) were mitochondrial proteins. The family of fatty-acid-binding proteins (FABPs) is specialized for different type of lipid responses in cells (Furuhashi and Hotamisligil, 2008), but their distinctive role in HCTs remains to be investigated. Interestingly, while FABP1 was the most abundant protein in HCs, we observed high levels of FABP4 and FABP5 in the LSECs and HSCs. The latter two family members were also among the top 10 most abundant proteins in adipocytes (Humphrey et al., 2013). FABP4 has recently been identified as an adipokine that can regulate insulin secretion during obesity by signaling to pancreatic β cells (Wu et al., 2014). Given the important role of the liver in whole-body metabolic homeostasis, and the recently identified capacity of the liver to regulate insulin sensitivity by the secretion of so called "hepatokines" (Misu et al., 2010), it is intriguing to speculate whether the vast abundance of FABP4

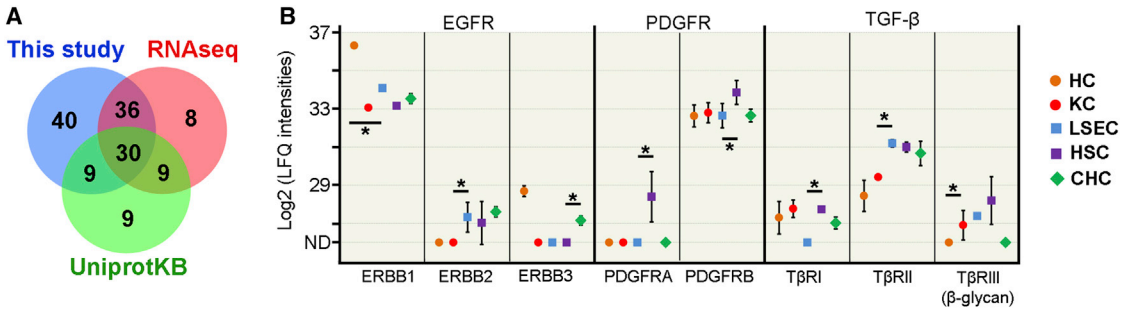

Figure 7. Quantitative Comparison of GF Receptors Levels in HCTs

(A) Venn diagram of identified hepatic GF receptors in this study (blue), RNASeq data from Mortazavi et al. (2008) (RPKM cutoff > 1; red), and the UniProtKB database (green).

(B) Protein expression profiles of HCTs were compared for EGFR, PDGFR, TGF-β, and VEGFR (median ± SD). Stars indicate t test significances (*p < 0.05). "ND" indicates "Not Detected."

in these hepatic cell types might also point to a hepatokine role of this molecule. Therefore, the approach we have applied here is likely to also prove valuable in the identification of key proteins in other organs and in the context of disease.

Remarkably, in view of previous concerns about limited coverage of proteomic data sets, our investigation showed the most complete coverage of receptor proteins compared to hepatic proteins of UniProtKB and a liver RNASeq analysis (Mortazavi et al., 2008). There were 26 receptors that were exclusively identified in the liver in UniProtKB and the RNA-seq data. However, since these are also highly represented in the blood, plasma, and platelets GeneCards database (Stelzer et al., 2011), these are likely to represent contamination of liver samples with blood proteins (Table S9).

The analysis of GF receptors expression in liver explains how individual HCTs selectively respond to various GF stimulations (Figure 7; Tables S1 and S9). For example, we detected PDGFRA receptor only in HSCs, and therefore, our data suggest that only these cells can display the PDGFRA/A and PDGFRA/B receptor dimers and respond to PDGF-AA and PDGF-CC GF signals in the liver (Boor et al., 2007). Since many of these receptors are involved in cellular crosstalk (Bohm et al., 2010; Taub, 2004), our quantitative data can contribute to elucidating complex intercellular events at the level of receptors and ligands.

Here we have employed advanced MS-based approaches to accurately determine the proteomic signatures of HCTs. Understanding the proteomic entities of hepatic cell populations improves our knowledge of liver function and has wide applications in basic research, biotechnology, and clinical diagnosis. Furthermore, our study provides a framework that can now be applied to altered physiological states of this or other organs.

EXPERIMENTAL PROCEDURES

Reagents

Peristaltic pump P1 was from GE Healthcare. Cell strainers were from BD Biosciences. Percoll, Collagenase IV, Pronase E, hyaluronidase, and DNase I were from Sigma (Germany). BSA was from Serva Electrophoresis. TrypLE was from Life Technologies. Magnetic-activated cell sorting (MACS) large cell columns, CD11b-, CD146 (LSEC)-, streptavidin- MicroBeads, and FcR Blocking Reagent were from Miltenyi Biotec. Nycodenz was from Progen Biotechnik. HCs staining with ASGPR1 was not included in the final version of this manuscript. The following antibodies were used for flow Cytometry: CD11b-APC/-FITC, CD146-APC/-FITC, EpCAM-APC/-FITC, and EpCAM-Biotin (Miltenyi Biotec); F4/80-Alex448 and all of the isotype Controls were from eBioscience. Hep-53.4 and J774.2 cell lines were purchased from Cell Lines Service (CLS, Germany). RT-PCR was performed according to manufacturer's guidelines (Supplemental Experimental Procedures).

Liver Perfusion and Isolation of HCTs

Male C57BL/6J mice (8–10 weeks old) were used for the isolation of HCTs. Mice were treated in accordance with approved protocol by Animal Protection Institute of Upper Bavaria (license number 2532.3-32-12). HCTs were isolated with different protocols according to their particular density and immunogenic properties (Figure 1A; Supplemental Experimental Procedures). The isolation of HCTs and their MS analysis were performed in quadruplicates (four independent biological replicates). The proteome comparison of freshly isolated HC versus Hepa 1-6 cell line and cultured primary HCs were performed in biological triplicates. For each biological replicate, three to five livers were used.

Sample Preparation for MS analysis

Cell lysis, protein digestion, and peptide fractionation were performed as previously described (Kulak et al., 2014). Briefly, samples were homogenized and lysed in StageTips with guanidinium hydrochloride buffer. Proteins were digested with Trypsin and Lys-C at 37°C overnight, and the resulting peptides were fractionated by SCX with six fractions for each SCX experiment. Hepa 1-6, Hep-53.4, and J774.2 cell lines were analyzed in parallel to generate a "peptide library" through the transfer of peptide identifications between measurements using the "match between runs" feature implemented in MaxQuant (Cox and Mann, 2008). The cell lines and primary HC were cultured in Dulbecco's modified Eagle's medium, supplemented with 10% FCS, 100 U/ml penicillin, and 100 ug/ml streptomycin. The collagen-coated plates were used for cell culture of primary HCs. Cells were harvested from about 80% confluent cultures using trypsin/EDTA and washed with PBS.

LC-MS/MS Analysis

Chromatographic peptide separation was performed with 50 cm columns packed in-house with ReproSil-Pur C18-AQ 1.9 μm resin (Dr. Maisch GmbH). Column temperature was maintained at 50°C by a homemade column oven. Peptide mixtures were analyzed by a Q-Exactive mass spectrometer (Thermo Fisher Scientific) coupled to an EASY-nLC 1000 UHPLC system (Thermo Fisher Scientific) via a nanoelectrospray ion source. Peptides were loaded in buffer A (0.1% formic acid) and eluted with a 240 min gradient of 5%–60% buffer B (80% acetonitrile and 0.1% Formic acid). MS data were obtained by one full scan and up to five data-dependent MS/MS scans. The full-scan MS spectra (300 to 1,750 m/z) were acquired with a resolution of 70,000 at m/z 200, a maximum injection time of 20 ms, and a target value of 3×10^6 charges. The precursors were isolated from a 2.2 m/z window, fixed first mass of 100 m/z, and fragmented by higher energy collisional dissociation (collision

energy 25). MS/MS spectra were acquired with a resolution of 17,500 at m/z 200, a maximum injection time of 120 ms, and a target value of 1e5 charges.

Data Analysis

Raw MS data (162 files) were processed by MaxQuant (1.4.1.4) with FDR < 0.01 at the level of both proteins and peptides (Cox and Mann, 2008). Peak lists were searched against the Mouse UniProt FASTA database (2/25/2012) containing 54,232 entries. Proteins and peptides (minimum seven amino acids) were identified using a target-decoy approach with a reversed database. Quantification of peptides and proteins was performed by MaxQuant with default settings. Bioinformatics analysis was performed with Perseus, Microsoft Excel, and R statistical computing software. Data and error bars are median ± SD. All annotations were extracted from UniProtKB. Categorical annotations were gene ontology (GO) biological process (BP), molecular function (MF), cellular component (CC), and KEGG pathway databases.

ACCESSION NUMBERS

All raw data and the MaxQuant output tables have been deposited to proteomeXchange (Vizcaíno et al., 2013) and can be accessed with the accession PXD000867. Please visit http://www.ebi.ac.uk/pride/archive/projects/PXD000867 to access the data.

SUPPLEMENTAL INFORMATION

Supplemental Information includes five figures, nine tables, and Supplemental Experimental Procedures and can be found with this article online at http://dx.doi.org/10.1016/j.cmet.2014.11.002.

ACKNOWLEDGMENTS

This work was funded by the Max Planck Society for the Advancement of Science and The Virtual Liver Network (grant 0315748) of the German Federal Ministry of Education and Research (BMBF).

Received: June 25, 2014
Revised: September 11, 2014
Accepted: November 4, 2014
Published: December 2, 2014

REFERENCES

Aebersold, R., and Mann, M. (2003). Mass spectrometry-based proteomics. Nature *422*, 198–207.

Beauvoit, B., Kitai, T., and Chance, B. (1994). Contribution of the mitochondrial compartment to the optical properties of the rat liver: a theoretical and practical approach. Biophys. J. *67*, 2501–2510.

Bohm, F., Kohler, U.A., Speicher, T., and Werner, S. (2010). Regulation of liver regeneration by growth factors and cytokines. EMBO Mol. Med. *2*, 294–305.

Boor, P., Sebekova, K., Ostendorf, T., and Floege, J. (2007). Treatment targets in renal fibrosis. Nephrol. Dial. Transplant *22*, 3391–3407.

Cox, J., and Mann, M. (2008). MaxQuant enables high peptide identification rates, individualized p.p.b.-range mass accuracies and proteome-wide protein quantification. Nat. Biotechnol. *26*, 1367–1372.

Cox, J., Neuhauser, N., Michalski, A., Scheltema, R.A., Olsen, J.V., and Mann, M. (2011). Andromeda: a peptide search engine integrated into the MaxQuant environment. J. Proteome Res. *10*, 1794–1805.

Cox, J., Hein, M.Y., Luber, C.A., Paron, I., Nagaraj, N., and Mann, M. (2014). Accurate proteome-wide label-free quantification by delayed normalization and maximal peptide ratio extraction, termed MaxLFQ. Mol. Cell. Proteomics *13*, 2513–2526.

Date, M., Matsuzaki, K., Matsushita, M., Tahashi, Y., Furukawa, F., and Inoue, K. (2000). Modulation of transforming growth factor beta function in hepatocytes and hepatic stellate cells in rat liver injury. Gut *46*, 719–724.

Elvevold, K., Smedsrød, B., and Martinez, I. (2008). The liver sinusoidal endothelial cell: a cell type of controversial and confusing identity. Am. J. Physiol. Gastrointest. Liver Physiol. *294*, G391–G400.

Ezkurdia, I., Vázquez, J., Valencia, A., and Tress, M. (2014). Analyzing the First Drafts of the Human Proteome. J. Proteome Res. . Published online July 16, 2014.

Falcón-Pérez, J.M., Lu, S.C., and Mato, J.M. (2010). Sub-proteome approach to the knowledge of liver. Proteomics Clin. Appl. *4*, 407–415.

Furuhashi, M., and Hotamisligil, G.S. (2008). Fatty acid-binding proteins: role in metabolic diseases and potential as drug targets. Nat. Rev. Drug Discov. *7*, 489–503.

Hannappel, E., and Huff, T. (2003). The thymosins. Prothymosin alpha, parathymosin, and beta-thymosins: structure and function. Vitam. Horm. *66*, 257–296.

Humphrey, S.J., Yang, G., Yang, P.Y., Fazakerley, D.J., Stöckli, J., Yang, J.Y., and James, D.E. (2013). Dynamic adipocyte phosphoproteome reveals that Akt directly regulates mTORC2. Cell Metab. *17*, 1009–1020.

Iida, M., Anna, C.H., Hartis, J., Bruno, M., Wetmore, B., Dubin, J.R., Sieber, S., Bennett, L., Cunningham, M.L., Paules, R.S., et al. (2003). Changes in global gene and protein expression during early mouse liver carcinogenesis induced by non-genotoxic model carcinogens oxazepam and Wyeth-14,643. Carcinogenesis *24*, 757–770.

Kim, M.S., Pinto, S.M., Getnet, D., Nirujogi, R.S., Manda, S.S., Chaerkady, R., Madugundu, A.K., Kelkar, D.S., Isserlin, R., Jain, S., et al. (2014). A draft map of the human proteome. Nature *509*, 575–581.

Kulak, N.A., Pichler, G., Paron, I., Nagaraj, N., and Mann, M. (2014). Minimal, encapsulated proteomic-sample processing applied to copy-number estimation in eukaryotic cells. Nat. Methods *11*, 319–324.

Larson, R.S., and Springer, T.A. (1990). Structure and function of leukocyte integrins. Immunol. Rev. *114*, 181–217.

Lee, S.M., Casey, C.A., and McVicker, B.L. (2009). Impact of asialoglycoprotein receptor deficiency on the development of liver injury. World J. Gastroenterol. *15*, 1194–1200.

Li, C., Hong, Y., Tan, Y.X., Zhou, H., Ai, J.H., Li, S.J., Zhang, L., Xia, Q.C., Wu, J.R., Wang, H.Y., and Zeng, R. (2004). Accurate qualitative and quantitative proteomic analysis of clinical hepatocellular carcinoma using laser capture microdissection coupled with isotope-coded affinity tag and two-dimensional liquid chromatography mass spectrometry. Mol. Cell. Proteomics *3*, 399–409.

Liu, W., Hou, Y., Chen, H., Wei, H., Lin, W., Li, J., Zhang, M., He, F., and Jiang, Y. (2011). Sample preparation method for isolation of single-cell types from mouse liver for proteomic studies. Proteomics *11*, 3556–3564.

Loser, K., Vogl, T., Voskort, M., Lueken, A., Kupas, V., Nacken, W., Klenner, L., Kuhn, A., Foell, D., Sorokin, L., et al. (2010). The Toll-like receptor 4 ligands Mrp8 and Mrp14 are crucial in the development of autoreactive CD8+ T cells. Nat. Med. *16*, 713–717.

Low, T.Y., van Heesch, S., van den Toorn, H., Giansanti, P., Cristobal, A., Toonen, P., Schafer, S., Hubner, N., van Breukelen, B., Mohammed, S., et al. (2013). Quantitative and qualitative proteome characteristics extracted from in-depth integrated genomics and proteomics analysis. Cell Rep. *5*, 1469–1478.

Magrane, M., and Consortium, U. (2011). UniProt Knowledgebase: a hub of integrated protein data. Database (Oxford). Published online March 29, 2011. http://dx.doi.org/10.1093/database/bar009.

Mann, M., Kulak, N.A., Nagaraj, N., and Cox, J. (2013). The coming age of complete, accurate, and ubiquitous proteomes. Mol. Cell *49*, 583–590.

Maschmeyer, P., Flach, M., and Winau, F. (2011). Seven steps to stellate cells. J. Vis. Exp. http://dx.doi.org/10.3791/2710.

Misu, H., Takamura, T., Takayama, H., Hayashi, H., Matsuzawa-Nagata, N., Kurita, S., Ishikura, K., Ando, H., Takeshita, Y., Ota, T., et al. (2010). A liver-derived secretory protein, selenoprotein P, causes insulin resistance. Cell Metab. *12*, 483–495.

Miyata, E., Masuya, M., Yoshida, S., Nakamura, S., Kato, K., Sugimoto, Y., Shibasaki, T., Yamamura, K., Ohishi, K., Nishii, K., et al. (2008). Hematopoietic origin of hepatic stellate cells in the adult liver. Blood *111*, 2427–2435.

Monetti, M., Nagaraj, N., Sharma, K., and Mann, M. (2011). Large-scale phosphosite quantification in tissues by a spike-in SILAC method. Nat. Methods *8*, 655–658.

Mortazavi, A., Williams, B.A., McCue, K., Schaeffer, L., and Wold, B. (2008). Mapping and quantifying mammalian transcriptomes by RNA-Seq. Nat. Methods *5*, 621–628.

Nagaraj, N., Wisniewski, J.R., Geiger, T., Cox, J., Kircher, M., Kelso, J., Pääbo, S., and Mann, M. (2011). Deep proteome and transcriptome mapping of a human cancer cell line. Mol. Syst. Biol. *7*, 548.

Okabe, M., Tsukahara, Y., Tanaka, M., Suzuki, K., Saito, S., Kamiya, Y., Tsujimura, T., Nakamura, K., and Miyajima, A. (2009). Potential hepatic stem cells reside in EpCAM+ cells of normal and injured mouse liver. Development *136*, 1951–1960.

Pan, C., Kumar, C., Bohl, S., Klingmueller, U., and Mann, M. (2009). Comparative proteomic phenotyping of cell lines and primary cells to assess preservation of cell type-specific functions. Mol. Cell. Proteomics *8*, 443–450.

Ramsköld, D., Wang, E.T., Burge, C.B., and Sandberg, R. (2009). An abundance of ubiquitously expressed genes revealed by tissue transcriptome sequence data. PLoS Comput. Biol. *5*, e1000598.

Ricklin, D., and Lambris, J.D. (2007). Complement-targeted therapeutics. Nat. Biotechnol. *25*, 1265–1275.

Röhrl, C., and Stangl, H. (2013). HDL endocytosis and resecretion. Biochim. Biophys. Acta *1831*, 1626–1633.

Schaab, C., Geiger, T., Stoehr, G., Cox, J., and Mann, M. (2012). Analysis of high accuracy, quantitative proteomics data in the MaxQB database. Mol. Cell. Proteomics *11*, http://dx.doi.org/10.1074/mcp.M111.014068.

Scheving, L.A., Zhang, L., Stevenson, M.C., Kwak, E.S., and Russell, W.E. (2006). The emergence of ErbB2 expression in cultured rat hepatocytes correlates with enhanced and diversified EGF-mediated signaling. Am. J. Physiol. Gastrointest. Liver Physiol. *291*, G16–G25.

Schwanhäusser, B., Busse, D., Li, N., Dittmar, G., Schuchhardt, J., Wolf, J., Chen, W., and Selbach, M. (2011). Global quantification of mammalian gene expression control. Nature *473*, 337–342.

Shi, R., Kumar, C., Zougman, A., Zhang, Y., Podtelejnikov, A., Cox, J., Wiśniewski, J.R., and Mann, M. (2007). Analysis of the mouse liver proteome using advanced mass spectrometry. J. Proteome Res. *6*, 2963–2972.

Stelzer, G., Dalah, I., Stein, T.I., Satanower, Y., Rosen, N., Nativ, N., Oz-Levi, D., Olender, T., Belinky, F., Bahir, I., et al. (2011). In-silico human genomics with GeneCards. Hum. Genomics *5*, 709–717.

Sulzmaier, F.J., Valmiki, M.K., Nelson, D.A., Caliva, M.J., Geerts, D., Matter, M.L., White, E.P., and Ramos, J.W. (2012). PEA-15 potentiates H-Ras-mediated epithelial cell transformation through phospholipase D. Oncogene *31*, 3547–3560.

Sun, A.H., Jiang, Y., Wang, X., Liu, Q.J., Zhong, F., He, Q.Y., Guan, W., Li, H., Sun, Y.L., Shi, L., et al. (2010). Liverbase: a comprehensive view of human liver biology. J. Proteome Res. *9*, 50–58.

Syal, G., Fausther, M., and Dranoff, J.A. (2012). Advances in cholangiocyte immunobiology. Am. J. Physiol. Gastrointest. Liver Physiol. *303*, G1077–G1086.

Taub, R. (2004). Liver regeneration: from myth to mechanism. Nat. Rev. Mol. Cell Biol. *5*, 836–847.

Thomson, A.W., and Knolle, P.A. (2010). Antigen-presenting cell function in the tolerogenic liver environment. Nat. Rev. Immunol. *10*, 753–766.

Tojkander, S., Gateva, G., and Lappalainen, P. (2012). Actin stress fibers—assembly, dynamics and biological roles. J. Cell Sci. *125*, 1855–1864.

Uhlen, M., Oksvold, P., Fagerberg, L., Lundberg, E., Jonasson, K., Forsberg, M., Zwahlen, M., Kampf, C., Wester, K., Hober, S., et al. (2010). Towards a knowledge-based Human Protein Atlas. Nat. Biotechnol. *28*, 1248–1250.

van't Veer, C., and van der Poll, T. (2008). Keeping blood clots at bay in sepsis. Nat. Med. *14*, 606–608.

Vizcaíno, J.A., Côté, R.G., Csordas, A., Dianes, J.A., Fabregat, A., Foster, J.M., Griss, J., Alpi, E., Birim, M., Contell, J., et al. (2013). The PRoteomics IDEntifications (PRIDE) database and associated tools: status in 2013. Nucleic Acids Res. *41* (Database issue), D1063–D1069.

Wilhelm, M., Schlegl, J., Hahne, H., Moghaddas Gholami, A., Lieberenz, M., Savitski, M.M., Ziegler, E., Butzmann, L., Gessulat, S., Marx, H., et al. (2014). Mass-spectrometry-based draft of the human proteome. Nature *509*, 582–587.

Wiśniewski, J.R., Hein, M.Y., Cox, J., and Mann, M. (2014). A 'proteomic ruler' for protein copy number and concentration estimation without spike-in standards. Mol. Cell. Proteomics. . Published online September 15, 2014.

Wu, L.E., Samocha-Bonet, D., Whitworth, P.T., Fazakerley, D.J., Turner, N., Biden, T.J., James, D.E., and Cantley, J. (2014). Identification of fatty acid binding protein 4 as an adipokine that regulates insulin secretion during obesity. Mol. Metab. *3*, 465–473.

Xia, X., Jung, D., Webb, P., Zhang, A., Zhang, B., Li, L., Ayers, S.D., Gabbi, C., Ueno, Y., Gustafsson, J.A., et al. (2012). Liver X receptor β and peroxisome proliferator-activated receptor δ regulate cholesterol transport in murine cholangiocytes. Hepatology *56*, 2288–2296.

Yan, W., Lee, H., Deutsch, E.W., Lazaro, C.A., Tang, W.L., Chen, E., Fausto, N., Katze, M.G., and Aebersold, R. (2004). A dataset of human liver proteins identified by protein profiling via isotope-coded affinity tag (ICAT) and tandem mass spectrometry. Mol. Cell. Proteomics *3*, 1039–1041.

Yin, C., Evason, K.J., Asahina, K., and Stainier, D.Y. (2013). Hepatic stellate cells in liver development, regeneration, and cancer. J. Clin. Invest. *123*, 1902–1910.